American Mineralogist, Volume 93, pages 548–557, 2008

Low-temperature calorimetric and magnetic data for natural end-members of the axinite group

Jan Filip,[1,2,*] Edgar Dachs,[3] Jiří Tuček,[1,4] Milan Novák,[2] and Petr Bezdička[5]

[1]Centre for Nanomaterial Research, Palacký University in Olomouc, Svobody 26, 771 46 Olomouc, Czech Republic
[2]Department of Geological Sciences, Masaryk University, Kotlářská 2, 611 37 Brno, Czech Republic
[3]Department of Material Engineering and Physics, University of Salzburg, Hellbrunnerstrasse 34, 5020 Salzburg, Austria
[4]Department of Experimental Physics, Palacký University in Olomouc, Svobody 26, 771 46 Olomouc, Czech Republic
[5]Institute of Inorganic Chemistry, Academy of Science of the Czech Republic, 250 68 Řež, Czech Republic

Abstract

The low-temperature heat capacities of natural near end-member minerals (about 95 mol%, except tinzenite of about 34 mol% on average) of the axinite group, previously characterized in detail by means of powder and single-crystal X-ray diffraction, electron microprobe, and Mössbauer spectroscopy, were measured by heat-pulse calorimetry using the Physical Properties Measurement System (Quantum Design) at temperatures between 5(2) and 300 K. From these data, the following entropy values [in J/(mol·K)] of the natural samples at 298.15 K were derived: $S_{298,\text{magnesioaxinite}} = 696.3 \pm 1.1$, $S_{298,\text{ferroaxinite}} = 743.5 \pm 3.5$, $S_{298,\text{manganaxinite}} = 737.5 \pm 2.6$, and $S_{298,\text{tinzenite}} = 758.1 \pm 2.8$. For the end-member compositions, the corrected heat capacities at 298.15 K and standard third-law entropies of the axinites are [all in J/(mol·K)]:

$C^{o}_{P\text{magnesioaxinite}} = 827.5 \pm 1.5$ and $S^{o}_{\text{magnesioaxinite}} = 693.7 \pm 1.1$,
$C^{o}_{P\text{ferroaxinite}} = 841.8 \pm 3.3$ and $S^{o}_{\text{ferroaxinite}} = 749.6 \pm 3.5$,
$C^{o}_{P\text{manganaxinite}} = 849.1 \pm 2.5$ and $S^{o}_{\text{manganaxinite}} = 737.8 \pm 2.6$, and
$C^{o}_{P\text{tinzenite}} = 841.6 \pm 2.6$, $S^{o}_{\text{tinzenite}} = 754.0 \pm 2.8$.

The standard entropies of manganaxinite and tinzenite include contributions of 1.9 and 4.3 J/(mol·K) for the range 0–5 K evaluated based on a Schottky anomaly fitted to the low-T C_P values of these axinites. The lowest measured heat capacities of ferroaxinite indicate that a lambda-type C_P anomaly should exist between 0 and 2 K. Its likely contribution to the standard entropy was estimated as ~5.2 J/(mol·K). A low-temperature C_P anomaly below 15 K for ferroaxinite is well-explained by ferromagnetic ordering, whereas for manganaxinite by uncompensated antiferromagnetic ordering, and for tinzenite by pure antiferromagnetic ordering.

Keywords: Axinite group minerals, chemical composition, heat capacity, heat-pulse calorimetry, magnetic ordering, low-temperature anomaly

Introduction

Minerals of the axinite group occur in Ca- and B-rich but relatively Al-poor environments including a variety of igneous, metamorphic, and hydrothermal rocks and mineral deposits (Pringle and Kawachi 1980; Dubé and Guha 1993; Novák and Filip 2002; Filip et al. 2006; for a comprehensive reference list of previous works see the review of Grew 1996). The general formula for the axinite-group minerals, $(Ca,Mn)_4(Fe,Mn,Mg)_2Al_4B_2Si_8O_{30}(OH)_2$, was proposed by Sanero and Gottardi (1968) and revised by Lumpkin and Ribbe (1979) and Andreozzi et al. (2004) in the form: $^{VI}[X1\ X2\ Y\ Z1\ Z2]_2{}^{IV}[T1\ T2\ T3\ T4\ T5]O_{30}(OH)_2$, where X1 = Ca (Na); X2 = Ca (Mn^{2+}); Y = Fe^{2+}, Mn^{2+}, Mg (Zn, Fe^{3+}, Al); Z1 = Al (Fe^{3+}); Z2 = Al; T1–T4 = Si and T5 = B (Si). The four presently known end-members of the axinite group are classified according to the divalent cation located in the X and Y sites: magnesioaxinite, ferroaxinite, and manganaxinite, all have 4 Ca atoms per formula unit (apfu) and Mg, Fe, or Mn in the Y site, respectively; whereas tinzenite has $2 \leq Ca \leq 4$ apfu and dominant Mn at both the X2 and Y sites (Milton et al. 1953; Sanero and Gottardi 1968; Basso et al. 1973; Lumpkin and Ribbe 1979; Belokoneva et al. 2001; Andreozzi et al. 2004; Filip et al. 2006). Perfect solid-solutions were observed between ferroaxinite and manganaxinite, and manganaxinite and tinzenite, and less commonly between ferroaxinite and magnesioaxinite. However, a miscibility gap between magnesioaxinite and manganaxinite does exist (Pringle and Kawachi 1980; Grew 1996; Andreozzi et al. 2000b). Ferroaxinite and Mg-poor manganaxinite are the most abundant compositions in nature (Grew 1996; Andreozzi et al. 2000b). The occurrences and associations of particular axinite group end-members were summarized by Ozaki (1972), Deer et al. (1997), and Grew (1996).

Axinite crystallizes in a $P\bar{1}$ space group and its structure is described as a sequence of layers of tetrahedrally and octahedrally coordinated cations. Tetrahedrally coordinated Si and B form isolated $B_2Si_8O_{30}$ planar clusters, whereas octahedrally coordinated cations build up sixfold finite chains Fe(Mn,Mg)-Al-Al-Al-Al-Fe(Mn,Mg) [i.e., Y-Z1-Z2-Z2-Z1-Y], laterally connected by highly distorted CaO_6 octahedra (Ito and Takéuchi 1952; Ito et al. 1969; Belokoneva et al. 1997, 2001; Andreozzi

* E-mail: jan.filip@upol.cz

et al. 2000a; Filip et al. 2006).

The chemical composition of axinite-group minerals has been correlated with their temperature of formation in low-grade regionally metamorphosed rocks and their relationship with tourmaline has been discussed (Pringle and Kawachi 1980; Dubé and Guha 1993; Novák and Filip 2002). However, for the quantitative understanding of the axinite formation and related thermodynamic calculations, an exact knowledge of thermodynamic properties is required. The necessary information is volume of each phase at a given *P* and *T*; heat capacity; entropy as a function of *T*; and enthalpy or Gibbs energy at some *P* and *T* (Anovitz and Hemingway 1996). The only experimental studies on axinite-group minerals were carried out by Khodakovsky et al. (see Anovitz and Hemingway 1996) and Mazdab et al. (1994), who reported heat-capacity functions and entropies for ferroaxinite and manganaxinite. However, these data are imperfect because a clear definition of the chemical composition of the particular samples examined was not given. Hence, the relevant data for axinite end-members are missing. In the last few decades, near end-member compositions for all minerals of the axinite group were described and characterized in detail (Basso et al. 1973; Belokoneva et al. 1997; Andreozzi et al. 2000a, 2004; Filip et al. 2006). This situation provides an unique opportunity for collection of high-quality thermochemical data relevant to all and well-defined near-end-members of the axinite group.

In this paper, we report the first low-temperature heat capacities measured on near-end-members of the axinite group at temperatures between 5(2) and 300 K. The heat-capacity data, corrected to the end-member compositions, have been used to calculate the standard third-law entropies of magnesioaxinite, ferroaxinite, manganaxinite, and tinzenite. Because heat capacity is complementary to magnetic properties, we also studied in detail the low-temperature magnetic properties of axinite-group minerals to fully describe the low-temperature heat-capacity anomalies. To the best of our knowledge, this is the first time where the low-temperature magnetic properties of axinite-group minerals are reported.

MATERIAL AND METHODS

Samples preparation and characterization

Well-characterized samples of axinite-group minerals—those closest to the end-member composition ever reported (except tinzenite)—were selected to obtain the most reliable thermodynamic data (Table 1): (1) gem-quality magnesioaxinite (with up to 96 mol% of the end-member) from the type locality at Merelani Hills, south Arusha, Tanzania, associated with diopside, zoisite, and grossular garnet in graphite-bearing pyroxene gneisses and marbles (Jobbins et al. 1975; Andreozzi et al. 2000a); (2) ferroaxinite (with up to 95 mol% of the end-member) from a contaminated pegmatite cutting the magnetite-rich portion of Fe-skarn body near Malešov, Czech Republic (Filip et al. 2006); (3) manganaxinite (with up to 95 mol% of the end-member) from axinite-quartz veins cutting quartz-piemontite rocks and metasediments enclosed in a volcanic rock sequence metamorphosed in prehnite-pumpellyite metamorphic facies from the Uchaly deposit, south Ural; and (4) tinzenite (~34 mol% of ideal tinzenite on average) from the type locality Fallota deposit in Switzerland (Belokoneva et al. 2001). In the case of the manganaxinite and tinzenite samples, quartz-axinite intergrowths were hand-picked and monomineral axinite samples were subsequently washed in a cold HCl to remove interstitial Fe-oxides and carbonates. Ferroaxinite and magnesioaxinite were available in the form of inclusion-free millimeter-sized crystals. Sample purity was checked by means of powder X-ray diffraction analysis and is estimated to be >99%.

Electron-microprobe analyses (EMPA) were performed using a CAMECA SX100 instrument under the following conditions: accelerating voltage of 15 kV, sample current of 10 nA, and a beam diameter of 5 μm. Sanidine (Si, Al, K), andradite (Ca, Fe), albite (Na), rhodonite (Mn), olivine (Mg), hornblende (Ti), fluorapatite (P), metallic V, and ZnS (Zn) were used as standards. Data were reduced using the X-phi routine (Merlet 1994). Chemical formulae of axinite end-members were calculated on the basis of 32 anions and from the stoichiometry B = 2, OH = 2 apfu.

TABLE 1. List of the studied samples and their Rietveld-refined cell parameters

Mineral Locality	magnesioaxinite* Merelani Hills, Tanzania	ferroaxinite† Malešov, Czech Rep.	manganaxinite Uchaly, Russia	tinzenite‡ Falotta, Switzerland
Source§	PB	U.K. 19288	BEL	BEL
Color	pale blue	violet	yellow	yellow
a (Å)	7.1415(4)	7.1512(4)	7.1765(4)	7.1703(7)
b (Å)	9.1663(5)	9.2038(5)	9.1901(5)	9.1458(11)
c (Å)	8.9440(5)	8.9599(5)	8.9711(5)	8.9624(8)
α (°)	91.905(4)	91.833(4)	91.824(3)	91.908(7)
β (°)	98.119(4)	98.177(4)	98.314(4)	98.709(9)
γ (°)	77.471(4)	77.317(4)	77.169(4)	77.087(8)
V (Å^3)	565.81	569.49	570.83	566.27

* Crystal structure described by Andreozzi et al. (2000a).
† Crystal structure described by Filip et al. (2006).
‡ Crystal structure described by Belokoneva et al. (2001).
§ PB = sample of P. Bongaerts; U.K. = Charles University in Prague, Czech Republic + catalog No.; BEL = sample of E.L. Belokoneva.

^{57}Fe transmission Mössbauer spectra of a powdered axinite sample were accumulated in a constant acceleration mode using a ^{57}Co in Rh source and 1024 channel detector at room temperature. Spectra were fitted by Lorentz functions using the computer program CONFIT2000 (Žák 2001). The isomer shift was calibrated with regard to an α-Fe foil. The percentages of Fe^{2+} and Fe^{3+} were established by measuring the integrated area of the respective doublets.

Powder X-ray diffraction was performed with a Siemens D5005 diffractometer (Bruker AXS, Germany) using a Ni-filtered Cu*K*α radiation (40 kV, 30 mA), diffracted beam monochromator and scintillation detector. X-ray patterns were measured in the range of 5 to 120 °2θ with a step of 0.02° and 15.5 s counting time per step. We used 1 mm divergence and anti-scatter slits and 0.1 mm detector slit. Quantitative analysis and unit-cell parameters calculation was performed with the MAUD software (Lutterotti et al. 1999).

Magnetic measurements were carried out with a superconducting quantum interference device (SQUID, Magnetic Properties Measurement System—MPMS XL-7, Quantum Design). The temperature dependence of the sample magnetization was measured from 2 to 298 K in an external magnetic field of 1000 Oe. The hysteresis loops were recorded in the temperature range of 2 to 50 K in external magnetic fields with intensities of up to 70 kOe.

Low-temperature calorimetry

Low-temperature heat capacities (C_P) were measured with a commercially designed calorimeter (heat capacity option of the Physical Properties Measurement System, PPMS, constructed by Quantum Design). The measurements were performed at temperatures between 5 and 300 K, and C_P was measured at 60 different temperatures and three times at each temperature on cooling with a logarithmic spacing. For ferroaxinite, an additional measurement was done in the temperature range 2–20 K. The axinites were either single crystals, directly placed on the sample platform of the calorimeter, or powders contained in hermetically sealed Al containers. The weights of the individual samples used varied between 6.3 and 35.6 mg. More details of the experimental method, as well as the data acquisition and evaluation procedures, including a discussion of data precision and accuracy for mineralogical samples, are given in Dachs and Bertoldi (2005) and Dachs and Geiger (2006).

Using the function "LinearFit" of the Experimental Data Analyst Package of Mathematica, the molar C_P data were then fitted to a C_P-polynomial of the general form $C_P = k_0 + k_1T^{-0.5} + k_2T^{-2} + k_3T^{-3} + k_4T + k_5T^2 + k_6T^3$. For this purpose, the data set was divided into three temperature regions, whereby each region was fitted individually, but a certain overlap was present. This procedure resulted in a good description of the experimental data (i.e., deviation usually <0.3%). The C_P of magnesioaxinite below 5 K was estimated from a plot of C_P/T vs. T^2 and a linear extrapolation to 0 K (i.e., $C_P = k_6T^3$). The C_P values of the Mn-bearing axinites below 5 K were estimated by first evaluating the lattice part of the heat capacity of these axinites and then fitting the difference $C_{P\,\mathrm{measured}} - C_{P\,\mathrm{lattice}}$ to a Schottky anomaly in a way similar to that performed by Dachs et al. (2007) in the case of Fe-Mg olivines. More details are given in Appendix A. For ferroaxinite, the heat-capacity data indicate a lambda-type C_P anomaly below 2 K, and its likely contribution to the standard

entropy of ferroaxinite was estimated by assuming a form as shown below.

As the natural axinites deviate from the theoretical end-member compositions (see below), we used PPMS-measured C_P values of pure natural quartz and periclase to correct for SiO_2 and MgO, PPMS-measured C_P of SRM-720 (standard reference material 720 "sapphir") to correct for Al_2O_3, and published low-temperature heat capacities of CaO, FeO, Fe_2O_3, and MnO to correct for those oxides (Grønvold and Westrum 1958; Gmelin 1969; Robie and Hemingway 1985; Stølen et al. 1996).

The calorimetric molar entropies of the axinites at 298.15 K, $S_{cal,298}$, were then determined by solving analytically and stepwise the integral:

$$S_{cal,298} = [S_{298} - S_0] = \int_0^{298.15} \frac{C_P}{T} \mathrm{d}T .$$

The uncertainty in $S_{cal,298}$ was determined as described previously (Dachs and Geiger 2006, Eqs. 5–9).

Results and discussion

Chemical composition and cell parameters of axinite end-members

All studied axinite samples, except tinzenite, are chemically homogeneous with compositions very close to the ideal stoichiometry. The results of the combination of EMPA and Mössbauer spectroscopy are given in Table 2 and Figure 1. The occupancy of Y and X2 sites depends on particular end-members; the only significant substitution in ferroaxinite, manganaxinite, and tinzenite is $Fe^{3+}Al_{-1}$ at the Z1 site (see Table 2 and Fig. 2). Other elements, not listed in Table 2, are below the detection limit of EMPA. In the case of magnesioaxinite, ferroaxinite, and tinzenite, the stoichiometric content of B is deduced from the T5 site volume (as reported by Andreozzi et al. 2000a; Belokoneva et al. 2001; Filip et al. 2006). Moreover, stoichiometric contents of both B and H were reported for magnesioaxinite from Tanzania on the basis of secondary ion mass spectroscopy (Andreozzi et al. 2000a). Our manganaxinite sample, which has not previously been studied by means of single-crystal X-ray diffraction, it has a chemical composition close to manganaxinite previously described by Belokoneva et al. (1997) and also by Andreozzi et al. (2004). Formula weights for all these samples are given in the Table 2.

The Rietveld-refined unit-cell parameters are given in Table 1. Slight differences from those derived from the crystal structure refinement (Andreozzi et al. 2000a; Belokoneva et al. 2001; Filip et al. 2006) are most probably caused by moderate variations of the chemical composition and, moreover, due to different methods employed. X-ray diffraction, used to detect possible impurities, revealed our samples to be impurity-free.

Table 2. Mean compositions and stoichiometry of axinite group minerals

	magnesioaxinite (n = 11)		ferroaxinite (n = 15)		manganaxinite (n = 11)		tinzenite (n = 13)	
	x	SD	x	SD	x	SD	x	SD
SiO_2 wt%	44.62	0.18	42.82	0.85	41.92	0.22	41.77	0.35
TiO_2	0.01	0.01	0.02	0.01	0.07	0.07	0.02	0.03
Al_2O_3	18.77	0.09	17.41	0.41	17.17	0.21	16.94	0.33
V_2O_3	0.05	0.04	n.d.	n.d.	0.01	0.01	0.03	0.03
CaO	21.18	0.16	19.61	0.18	18.23	0.46	16.19	2.29
MgO	7.22	0.09	0.21	0.08	0.23	0.10	0.21	0.05
FeO*	0.00	0.01	11.63	0.29	1.32	0.07	1.15	0.43
MnO	0.49	0.04	0.58	0.14	13.65	0.83	16.46	2.87
ZnO	0.02	0.02	n.d.	n.d.	0.02	0.02	0.02	0.02
Na_2O	0.02	0.02	0.01	0.01	0.02	0.01	0.02	0.03
K_2O	0.02	0.01	n.d.	n.d.	0.01	0.02	0.01	0.01
P_2O_5	0.02	0.02	n.d.	n.d.	0.02	0.02	0.02	0.01
B_2O_3†	6.48	0.02	6.12	0.04	6.08	0.04	6.05	0.04
H_2O†	1.67	0.01	1.59	0.01	1.57	0.01	1.57	0.01
Total	100.56	0.30	100.00	0.46	100.34	0.50	100.47	0.34
Si apfu	7.985	0.013	8.101	0.110	7.987	0.014	8.000	0.025
Ti	0.002	0.001	0.002	0.002	0.011	0.010	0.003	0.004
Al	3.960	0.023	3.883	0.111	3.856	0.028	3.823	0.056
V	0.007	0.006	–	–	0.002	0.001	0.005	0.005
Ca	4.060	0.029	3.975	0.041	3.721	0.087	3.321	0.456
Mg	1.926	0.020	0.060	0.021	0.065	0.028	0.059	0.015
Fe^{2+}‡	0.001§	0.001	1.803	0.051	0.053	0.003	0.009	0.003
Fe^{3+}‡	–	–	0.037	0.001	0.158	0.009	0.175	0.066
Mn	0.074	0.007	0.093	0.022	2.204	0.138	2.673	0.481
Zn	0.002	0.002	–	–	0.003	0.003	0.002	0.003
Na	0.007	0.007	0.004	0.005	0.006	0.005	0.009	0.012
K	0.004	0.003	–	–	0.003	0.004	0.002	0.002
P	0.004	0.003	–	–	0.003	0.003	0.003	0.002
B	1.998	0.002	2.000	0.000	2.000	0.000	2.000	0.000
H	2.000	0.000	2.000	0.000	2.000	0.000	2.000	0.000
Σ cations	20.028	0.010	19.957	0.060	20.073	0.014	20.084	0.036
Molar weight	1081.17	0.69	1136.66	3.25	1148.75	3.00	1156.06	7.92

Note: n.d. = not determined; n = number of electron microprobe analyses; x = mean result of analyses; SD = standard deviation (1σ).
* All Fe as FeO.
† Calculated from stoichiometry.
‡ Ratio Fe^{3+}/Fe^{2+} determined by Mössbauer spectroscopy.
§ All Fe as Fe^{2+}.

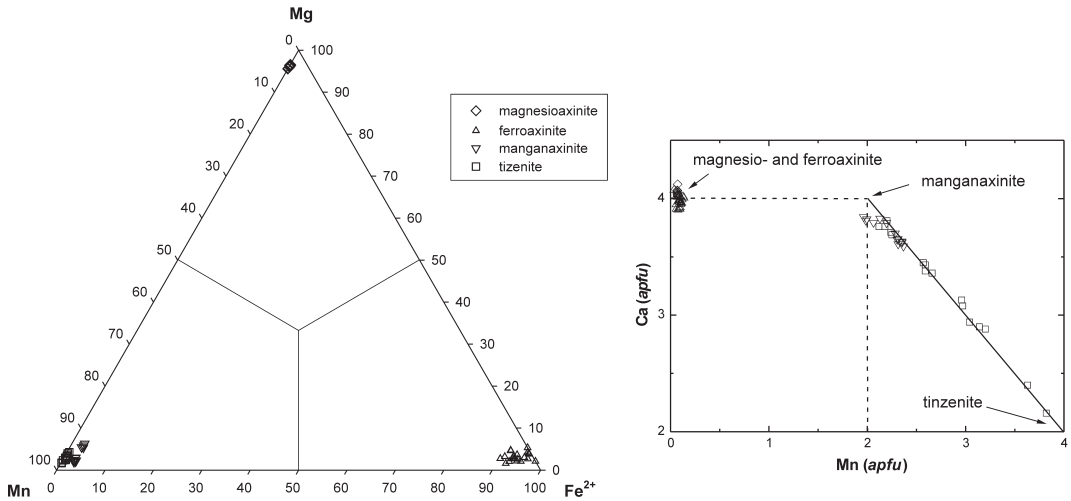

Figure 1. Chemical compositions of axinite-group minerals. Symbols represent electron microprobe analyses on crystals selected for this study.

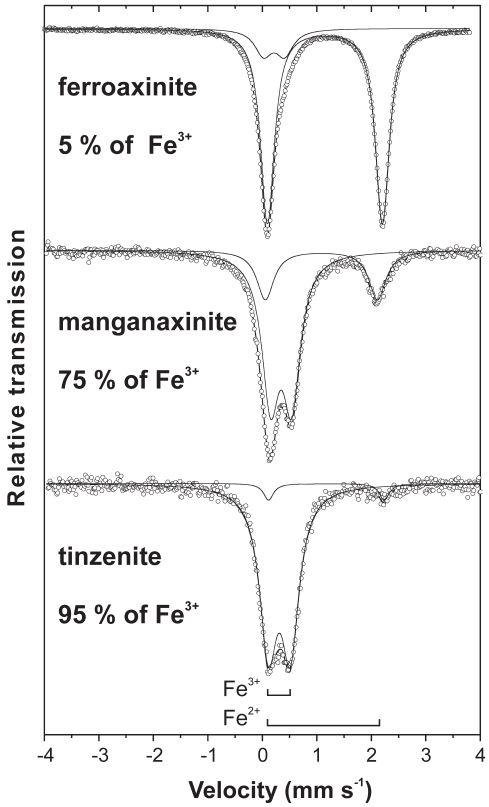

FIGURE 2. Room-temperature ^{57}Fe Mössbauer spectra of axinite-group minerals (except Fe-free magnesioaxinite). Note, both Fe^{2+} and Fe^{3+} are in a high-spin state.

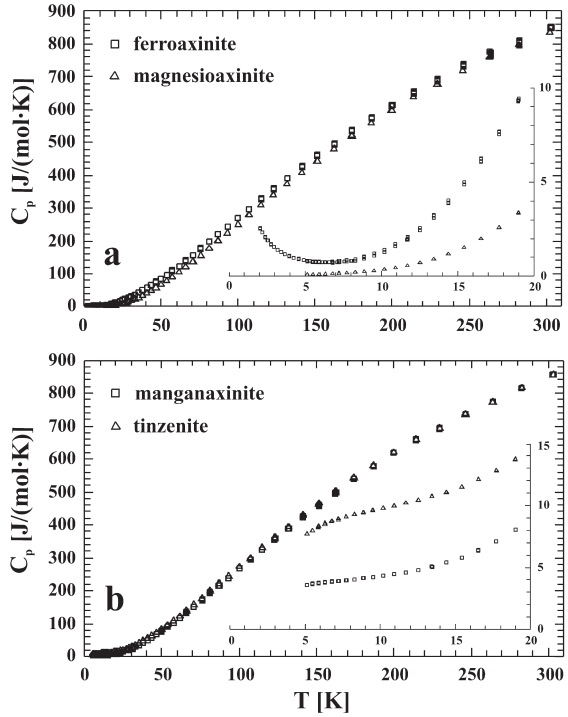

FIGURE 3. Temperature dependence of the heat capacity of axinite-group minerals. Low-temperature regions in the range 0–12 K are inserted. (**a**) Data for end-member ferroaxinite and magnesioaxinite. (**b**) Data for manganaxinite and tinzenite.

Heat capacity and standard entropy of axinite group minerals

The low-temperature PPMS measurements of natural end-members of the axinite group are given in Appendix B[1]. The low-temperature C_P values of magnesioaxinite and ferroaxinite are shown in Figure 3a, and those of manganaxinite and tinzenite in Figure 3b. The low-temperature regions are plotted in separate insets of these figures. Magnetic effects are visible for the Fe- and Mn-bearing axinites: for ferroaxinite, the C_P values at very low T run through a minimum around 6 K increasing to values of ~2.6 J/(mol·K) at 2 K, indicating that a magnetic-ordering transition of a possible form, as shown in Figure 4, must exist between 0 and 2 K (see below). The Mn-bearing axinites have anomalously high C_P values at 5 K [3.6 J/(mol·K) for manganaxinite and 7.7 J/(mol·K) for tinzenite], with a concave shape of the C_P-T data between 5 and ~12 K, possibly related to a Schottky-like C_P anomaly and/or a magnetic-ordering transition. For manganaxinite and tinzenite, the extrapolation of C_P in the temperature range 0–5 K has been done on the basis of a Schottky anomaly (see Appendix A and Fig. 4 for more details); for ferroaxinite a lambda-type C_P anomaly between 0 and 2 K with a peak at around 1 K was assumed (Fig. 4). The contributions of these regions to the standard entropies amount to 1.9 and 4.3 J/(mol·K) for manganaxinite and tinzenite, and to 5.2 J/(mol·K) for ferroaxinite, respectively, and are included in the standard entropy values given in Tables 3a and 3b. Other heat-capacity anomalies at higher temperatures have not been observed.

The integration of the C_P/T-T data yields the following calorimetric entropies [all in J/(mol·K)] at 298.15 K for the natural axinites: $S_{cal,298,magnesioaxinite} = 696.3 \pm 1.1$, $S_{cal,298,ferroaxinite} = 743.5 \pm 3.5$, $S_{cal,298,manganaxinite} = 737.5 \pm 2.6$, and $S_{cal,298,tinzenite} = 758.1 \pm 2.8$. Based on the crystal-chemical data given in Table 2, the following corrections have been made to the measured C_P values of the natural axinites, to derive low-temperature heat capacities of the pure end-members:

$$C_P^{corr} = C_P^{meas} + 0.015C_P^{SiO_2} + 0.02C_P^{Al_2O_3} - 0.06C_P^{CaO} + 0.074C_P^{MgO} - 0.074C_P^{MnO} \text{ (magnesioaxinite)},$$

$$C_P^{corr} = C_P^{meas} - 0.101C_P^{SiO_2} + 0.0585C_P^{Al_2O_3} + 0.025C_P^{CaO} - 0.06C_P^{MgO} + 0.197C_P^{FeO} - 0.019C_P^{Fe_2O_3} - 0.093C_P^{MnO} \text{ (ferroaxinite)},$$

$$C_P^{corr} = C_P^{meas} + 0.13C_P^{SiO_2} + 0.072C_P^{Al_2O_3} + 0.279C_P^{CaO} - 0.065C_P^{MgO} - 0.053C_P^{FeO} - 0.158C_P^{Fe_2O_3} - 0.204C_P^{MnO} \text{ (manganaxinite)},$$

$$C_P^{corr} = C_P^{meas} + 0.0885C_P^{Al_2O_3} - 0.059C_P^{MgO} - 0.009C_P^{FeO} - 0.175C_P^{Fe_2O_3} \text{ (tinzenite)}.$$

From these data, the following heat capacities at 298.15 K and standard third-law entropies of the end-members of the axinite group were derived [all in J/(mol·K)]:

[1] Deposit item AM-08-013, Appendix B (a low-temperature PPMS measurement of natural end-members of axinite-group). Deposit items are available in two ways: For a paper copy contact the Business Office of the Mineralogical Society of America (see inside front cover of recent issue) for price information. For an electronic copy visit the MSA web site at http://www.minsocam.org, go to the American Mineralogist Contents, find the table of contents for the specific volume/issue wanted, and then click on the deposit link there.

$C_{P\,\mathrm{magnesioaxinite}}^{\circ} = 827.5 \pm 1.5$ and $S_{\mathrm{magnesioaxinite}}^{\circ} = 693.7 \pm 1.1$,
$C_{P\,\mathrm{ferroaxinite}}^{\circ} = 841.8 \pm 3.3$ and $S_{\mathrm{ferroaxinite}}^{\circ} = 749.6 \pm 3.5$,
$C_{P\,\mathrm{manganaxinite}}^{\circ} = 849.1 \pm 2.5$ and $S_{\mathrm{manganaxinite}}^{\circ} = 737.8 \pm 2.6$,
and
$C_{P\,\mathrm{tinzenite}}^{\circ} = 841.6 \pm 2.6$ $S_{\mathrm{tinzenite}}^{\circ} = 754.0 \pm 2.8$.

Tables 3a and 3b summarize standard thermodynamic functions of axinite group end-members at selected temperatures between 5 and 298.15 K.

Generally, our calorimetric data for C_P° and the derived S° are lower than literature values. The best agreement between our data and the published thermochemical data and estimates is for manganaxinite. For manganaxinites, the calorimetric C_P° value is only 0.6% [absolute 5.1 J/(mol·K)] lower than the literature value of 854.2 ± 1.8 J/(mol·K) (Mazdab et al. 1994), and the standard entropy value of 737.8 ± 2.6 J/(mol·K) is about 1.3% lower than the literature value of 747.2 ± 1.6 J/(mol·K) (Mazdab et al. 1994). For ferroaxinite, the discrepancies increase slightly, and C_P° and S° derived herein are 2.2 and 1.5% lower for this end-member, for which the literature data are 861.0 ± 1.8 J/(mol·K) (Mazdab et al. 1994) and 761.4 ± 1.6 J/(mol·K) for C_P° and S°, respectively (Mazdab et al. 1994), but only 0.8% lower than published entropy of $S_{\mathrm{ferroaxinite}}^{\circ}$ = 755.6 ± 8.4 J/(mol·K) (in Khodakovsky et al., see Anovitz and Hemingway 1996). The reason may be due to the use of samples in previous works with inadequately known composition, most probably far different from end-member composition.

Magnetic ordering and magnetic contributions to the low-temperature heat capacities of axinite-group minerals

The low-temperature heat-capacity measurements revealed various unspecified magnetic effects in the case of Fe- and Mn-bearing axinites. To understand the low-temperature magnetic regime of axinite-group minerals, a series of magnetic measurements, including the temperature dependence of the magnetic mass susceptibility (χ) and hysteresis loops at various temperatures, were performed. The measured data for the three samples are depicted in Figures 5 and 6. With respect to the bulk character of the C_P data discussed above, we also report on the magnetic properties from their macroscopic manifestations.

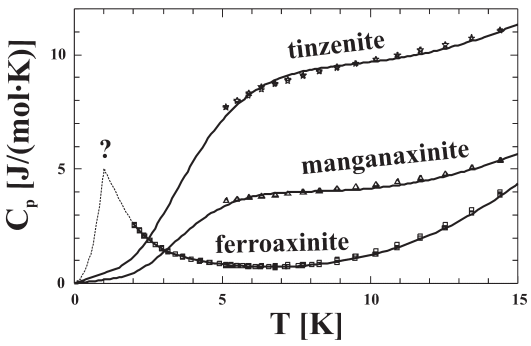

FIGURE 4. Heat capacity of ferroaxinite, manganaxinite, and tinzenite in the low-temperature region 0–15 K and functions used to extrapolate C_P to 0 K. For manganaxinite and tinzenite, this extrapolation is done in the temperature range 0–5 K on the basis of a Schottky anomaly (solid curves, representing $C_{P\,\mathrm{lattice}} + C_{P\,\mathrm{Schottky}}$); for ferroaxinite, a lambda-type C_P anomaly between 0 and 2 K with a peak at around 1 K was assumed as indicated by the stippled curve.

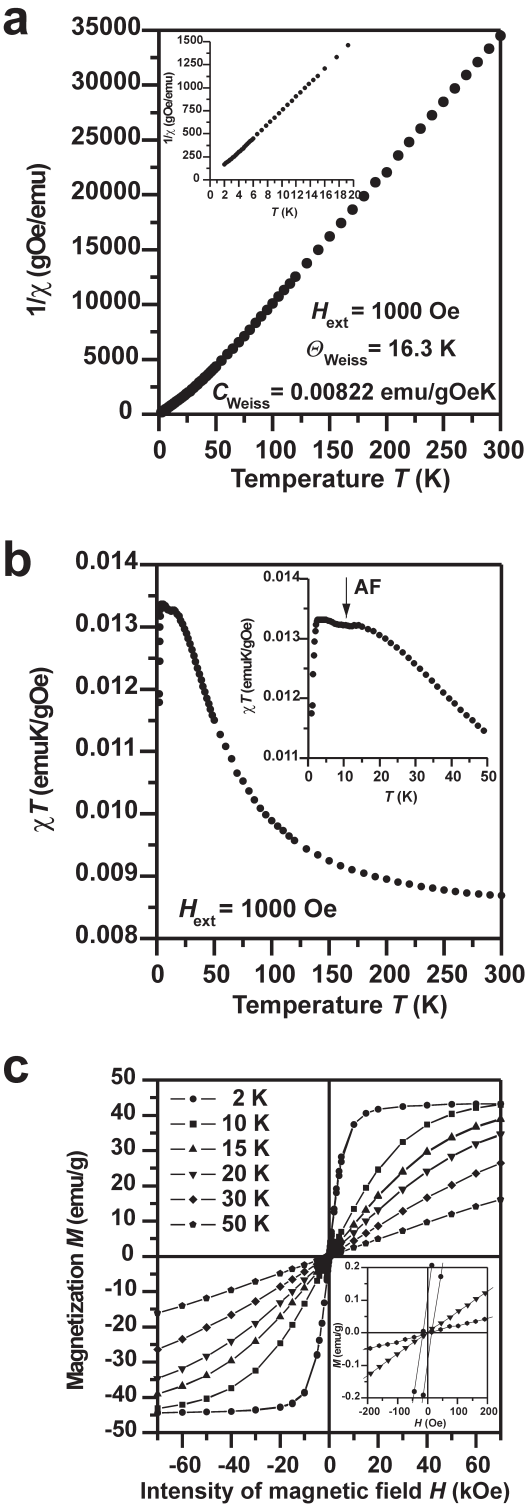

FIGURE 5. The results of magnetic measurements of ferroaxinite. (**a**) Inverse temperature dependence of magnetic mass susceptibility (χ) with an inset of low-temperature region 0–20 K. (**b**) Plot of χT vs. T with an inset of low-temperature region 0–50 K (AF = arrow points to the temperature where antiferromagnetic interactions contribute to ferroaxinite magnetic ordering). (**c**) Field dependence of the magnetization at selected temperatures with an inset of the hysteresis loop near the origin.

TABLE 3A. Molar thermodynamic functions of ferroaxinite and magnesioaxinite at selected temperatures between 2 and 298.15 K

	ferroaxinite (M = 1140.24 g/mol)				magnesioaxinite (M = 1077.14 g/mol)			
T (K)	$C_{P,m}$ [J/(K·mol)]	ΔT_0S_m* [J/(K·mol)]	$\Delta T_0H_m/T$* [J/(K·mol)]	Φ_m* [J/(K·mol)]	$C_{P,m}$ [J/(K·mol)]	ΔT_0S_m [J/(K·mol)]	$\Delta T_0H_m/T$ [J/(K·mol)]	Φ_m [J/(K·mol)]
2	2.4454	5.1449	2.6658	2.4791				
3	1.5046	5.9598	2.4347	3.5251				
4	1.0538	6.3221	2.1382	4.1839				
5	0.8420	6.5318	1.8977	4.6341	0.0816	0.0275	0.0205	0.0070
6	0.7457	6.6754	1.7124	4.9629	0.1089	0.0450	0.0332	0.0119
7	0.7352	6.7885	1.5726	5.2159	0.1406	0.0641	0.0461	0.0179
8	0.8087	6.8905	1.4716	5.4189	0.1838	0.0855	0.0605	0.0250
9	0.9732	6.9943	1.4062	5.5881	0.2416	0.1103	0.0773	0.0331
10	1.238	7.110	1.375	5.734	0.320	0.140	0.097	0.042
11	1.612	7.244	1.379	5.865	0.425	0.175	0.122	0.053
12	2.105	7.405	1.418	5.987	0.566	0.218	0.153	0.065
13	2.725	7.597	1.494	6.103	0.751	0.270	0.192	0.078
14	3.481	7.826	1.608	6.218	0.988	0.334	0.240	0.094
15	4.381	8.096	1.762	6.334	1.285	0.412	0.299	0.113
16	5.392	8.410	1.957	6.453	1.649	0.506	0.372	0.134
17	6.520	8.770	2.192	6.579	2.087	0.619	0.459	0.159
18	7.775	9.178	2.466	6.712	2.605	0.752	0.564	0.188
19	9.142	9.635	2.781	6.853	3.211	0.909	0.687	0.222
20	10.609	10.140	3.136	7.005	3.911	1.091	0.830	0.261
25	19.223	13.396	5.459	7.938	8.934	2.456	1.906	0.550
30	29.630	17.796	8.597	9.199	16.433	4.712	3.670	1.042
35	41.551	23.241	12.437	10.804	26.156	7.948	6.163	1.786
40	54.79	29.64	16.89	12.75	37.81	12.18	9.37	2.81
45	69.18	36.91	21.89	15.02	51.09	17.39	13.26	4.13
50	84.59	44.99	27.38	17.61	65.73	23.52	17.76	5.76
55	100.90	53.81	33.32	20.49	81.51	30.51	22.83	7.68
60	117.98	63.32	39.66	23.66	98.21	38.32	28.41	9.91
70	154.06	84.18	53.40	30.79	133.74	56.09	40.89	15.20
80	192.04	107.22	68.34	38.88	171.26	76.38	54.83	21.56
90	231.16	132.09	84.25	47.84	209.95	98.78	69.91	28.87
100	270.71	158.49	100.92	57.57	249.18	122.93	85.87	37.06
110	309.99	186.14	118.14	68.00	288.41	148.52	102.50	46.02
120	348.30	214.76	135.73	79.03	327.20	175.28	119.61	55.67
130	384.97	244.10	153.51	90.59	365.16	202.98	137.05	65.93
140	421.43	273.97	171.34	102.62	401.92	231.39	154.66	76.73
150	457.12	304.27	189.21	115.05	437.26	260.33	172.33	88.00
160	491.62	334.88	207.04	127.84	471.81	289.66	189.97	99.69
170	524.79	365.68	224.76	140.92	505.28	319.27	207.54	111.73
180	556.59	396.59	242.32	154.26	537.51	349.07	224.98	124.09
190	587.01	427.50	259.67	167.83	568.42	378.97	242.25	136.72
200	616.09	458.35	276.77	181.59	598.01	408.88	259.30	149.58
210	643.86	489.09	293.59	195.50	626.30	438.75	276.11	162.64
220	670.39	519.66	310.12	209.54	653.32	468.51	292.65	175.86
230	695.74	550.02	326.34	223.68	679.13	498.13	308.89	189.23
240	719.96	580.15	342.24	237.91	703.79	527.56	324.84	202.72
250	743.13	610.01	357.82	252.20	727.36	556.77	340.47	216.30
260	765.31	639.59	373.07	266.53	749.90	585.74	355.79	229.95
270	786.55	668.88	387.99	280.89	771.47	614.45	370.79	243.66
273.15	793.05	678.04	392.62	285.42	778.08	623.43	375.45	247.99
280	806.90	697.85	402.59	295.27	792.13	642.88	385.47	257.41
290	826.43	726.51	416.87	309.64	811.94	671.02	399.84	271.19
298.15	841.76	749.63	428.28	321.35	827.48	693.74	411.31	282.43

Note: $\Phi_m \equiv \Delta T_0S_m - \Delta T_0H_m/T$.
* Note that a lambda-type C_P anomaly between 0 and 2 K, as depicted in Figure 4, was assumed for ferroaxinite.

Individual magnetic interactions among magnetically active ions can be derived under certain circumstances, but this could be unambiguous in the case of complex structure of axinite, and, moreover, it is beyond the scope of the present paper.

In the case of ferroaxinite, a ferromagnetic ordering at low temperatures was confirmed. From Figure 5a, one can observe that in a paramagnetic state (i.e., in a temperature interval from about 20 to 300 K), the inverse magnetic mass susceptibility of ferroaxinite adheres to the Curie-Weiss law $\chi(T) = C/(T - \Theta_{Weiss})$, where C is the Curie constant and Θ_{Weiss} stands for the Weiss temperature, which is generally recognized as an indication of the strength of the magnetic interactions in the materials. After fitting the experimental data with a straight line, we have arrived at Θ_{Weiss} = 16.3 K, which can be ascribed to a magnetic transition temperature. This result implies that below this temperature, the low-temperature magnetic regime of ferroaxinite is predominantly governed by magnetic interactions of a ferromagnetic nature that act between magnetically active ions. For the sake of clarity, a plot of χT vs. T has been constructed (see Fig. 5b) and at temperatures from 20 to 300 K, its profile resembles that expected for ferromagnetic materials for which the product of χT generally rises monotonously with decreasing temperature in the paramagnetic regime (Blundell 2001). Additionally, a hysteresis loop, perfectly saturating at 2 K, shows a magnetically ordered state with a coercive field of 16 Oe (see Fig. 5c). There is an evident decrease of hysteresis

TABLE 3B. Molar thermodynamic functions of manganaxinite and tinzenite at selected temperatures between 5 and 298.15 K

	manganaxinite (M = 1138.42 g/mol)				tinzenite (M = 1168.13 g/mol)			
T (K)	$C_{p,m}$ [J/(K·mol)]	ΔT_0S_m [J/(K·mol)]	$\Delta T_0H_m/T$ [J/(K·mol)]	Φ_m [J/(K·mol)]	$C_{p,m}$ [J/(K·mol)]	ΔT_0S_m [J/(K·mol)]	$\Delta T_0H_m/T$ [J/(K·mol)]	Φ_m [J/(K·mol)]
5	3.3358	1.8838	1.2176	0.6661	7.1649	4.2753	2.6758	1.5995
6	3.7483	2.5521	1.6261	0.9260	8.3398	5.7314	3.5627	2.1686
7	3.8725	3.1394	1.9383	1.2011	8.8277	7.0558	4.2821	2.7737
8	3.9856	3.6640	2.1872	1.4768	9.1886	8.2592	4.8738	3.3854
9	4.0971	4.1398	2.3932	1.7466	9.4807	9.3588	5.3699	3.9889
10	4.217	4.578	2.569	2.008	9.740	10.371	5.794	4.577
11	4.356	4.986	2.725	2.260	9.992	11.311	6.164	5.147
12	4.528	5.372	2.868	2.504	10.258	12.192	6.494	5.698
13	4.747	5.743	3.004	2.739	10.555	13.025	6.795	6.230
14	5.022	6.104	3.138	2.966	10.898	13.819	7.075	6.744
15	5.365	6.462	3.274	3.187	11.298	14.584	7.343	7.241
16	5.785	6.821	3.418	3.403	11.766	15.328	7.605	7.723
17	6.290	7.187	3.572	3.615	12.310	16.057	7.865	8.192
18	6.885	7.562	3.739	3.824	12.938	16.778	8.129	8.649
19	7.576	7.953	3.922	4.031	13.656	17.496	8.401	9.096
20	8.369	8.361	4.124	4.237	14.469	18.217	8.683	9.534
25	13.957	10.777	5.485	5.292	20.118	22.002	10.360	11.642
30	22.392	14.025	7.562	6.463	28.581	26.377	12.654	13.723
35	33.227	18.261	10.427	7.834	39.473	31.572	15.681	15.891
40	46.10	23.52	14.06	9.46	52.36	37.66	19.44	18.22
45	60.61	29.77	18.42	11.36	66.80	44.65	23.89	20.76
50	76.41	36.97	23.42	13.55	82.47	52.49	28.95	23.54
55	93.23	45.03	28.99	16.04	99.09	61.12	34.57	26.56
60	110.86	53.89	35.07	18.82	116.48	70.49	40.67	29.82
70	147.93	73.74	48.52	25.22	152.93	91.16	54.08	37.08
80	186.60	96.00	63.35	32.65	190.86	114.04	68.79	45.25
90	226.11	120.26	79.24	41.02	229.59	138.75	84.50	54.25
100	265.89	146.14	95.91	50.23	268.59	164.96	100.96	64.00
110	305.46	173.34	113.17	60.17	307.43	192.38	117.97	74.41
120	344.42	201.59	130.82	70.77	345.72	220.78	135.36	85.42
130	382.38	230.67	148.72	81.95	383.12	249.94	152.98	96.95
140	419.02	260.36	166.73	93.63	419.29	279.66	170.72	108.94
150	455.30	290.49	184.74	105.75	455.65	309.82	188.50	121.32
160	491.05	321.03	202.78	118.25	490.67	340.36	206.30	134.06
170	525.15	351.83	220.75	131.08	523.78	371.11	224.01	147.10
180	557.68	382.77	238.57	144.20	555.26	401.94	241.55	160.40
190	588.72	413.76	256.19	157.58	585.28	432.77	258.85	173.92
200	618.35	444.72	273.56	171.16	613.98	463.53	275.90	187.63
210	646.64	475.58	290.66	184.92	641.47	494.16	292.66	201.50
220	673.68	506.29	307.46	198.83	667.82	524.61	309.11	215.50
230	699.52	536.81	323.95	212.86	693.12	554.86	325.26	229.59
240	724.25	567.11	340.12	226.99	717.41	584.87	341.10	243.77
250	747.93	597.16	355.96	241.20	740.77	614.64	356.62	258.01
260	770.62	626.94	371.47	255.46	763.23	644.13	371.83	272.30
270	792.37	656.43	386.66	269.77	784.85	673.34	386.73	286.61
273.15	799.04	665.66	391.38	274.28	791.50	682.48	391.36	291.12
280	813.25	685.63	401.53	284.10	805.68	702.26	401.32	300.94
290	833.30	714.52	416.07	298.45	825.75	730.89	415.62	315.27
298.15	849.06	737.83	427.69	310.14	841.58	753.99	427.04	326.95

Note: $\Phi_m \equiv \Delta T_0S_m - \Delta T_0H_m/T$.

as the temperature is raised, and above 20 K, there is no observable hysteresis, indicating that ferroaxinite has entered the paramagnetic regime.

However, a closer inspection of the low-temperature profile of χT vs. T curve (see inset in Fig. 5b) shows a slight change of the trend in a temperature interval from 10 to 20 K. This result implies that at these temperatures, the strength of another magnetic interaction, being of antiferromagnetic nature, between magnetically active ions in the ferroaxinite structure has become similar to and/or higher than the ferromagnetic one that is dominant below 5 K. To assign the types of the magnetically active ions between which the magnetic interactions take place, we have compared the measured magnetic data to the structure of ferroaxinite. Thus, two significant magnetic pathways can be identified: (1) the ferromagnetic interaction between Fe^{2+} and Fe^{2+} ions (minimum distance of two nearest Y sites is 4.133 Å), and (2) the antiferromagnetic interaction between Fe^{2+} and neighboring Fe^{3+} ions (Y and Z1 site, respectively; distance of 3.212 Å) as the Fe^{3+} substitution into the Z1 site was confirmed by Mössbauer spectroscopy (see Fig. 2; Filip et al. 2006). Below 16 K, both interactions coexist and their strengths change as the temperature further decreases. At temperatures below 5 K, ferromagnetic interactions become stronger, thus establishing low-temperature ferromagnetic ordering of the magnetic moments within the ferroaxinite sample. At this stage, the presence of other magnetic interactions cannot be excluded (e.g., between Mn ions substituting into the Y site; see Table 2). However, we assume that they do not play a significant role on the resulting magnetic behavior of the studied ferroaxinite.

For manganaxinite, on the other hand, the calculated Weiss temperature is –8.9 K (see Fig. 6a, left). The negative value indicates that the dominant magnetic interaction is of antifer-

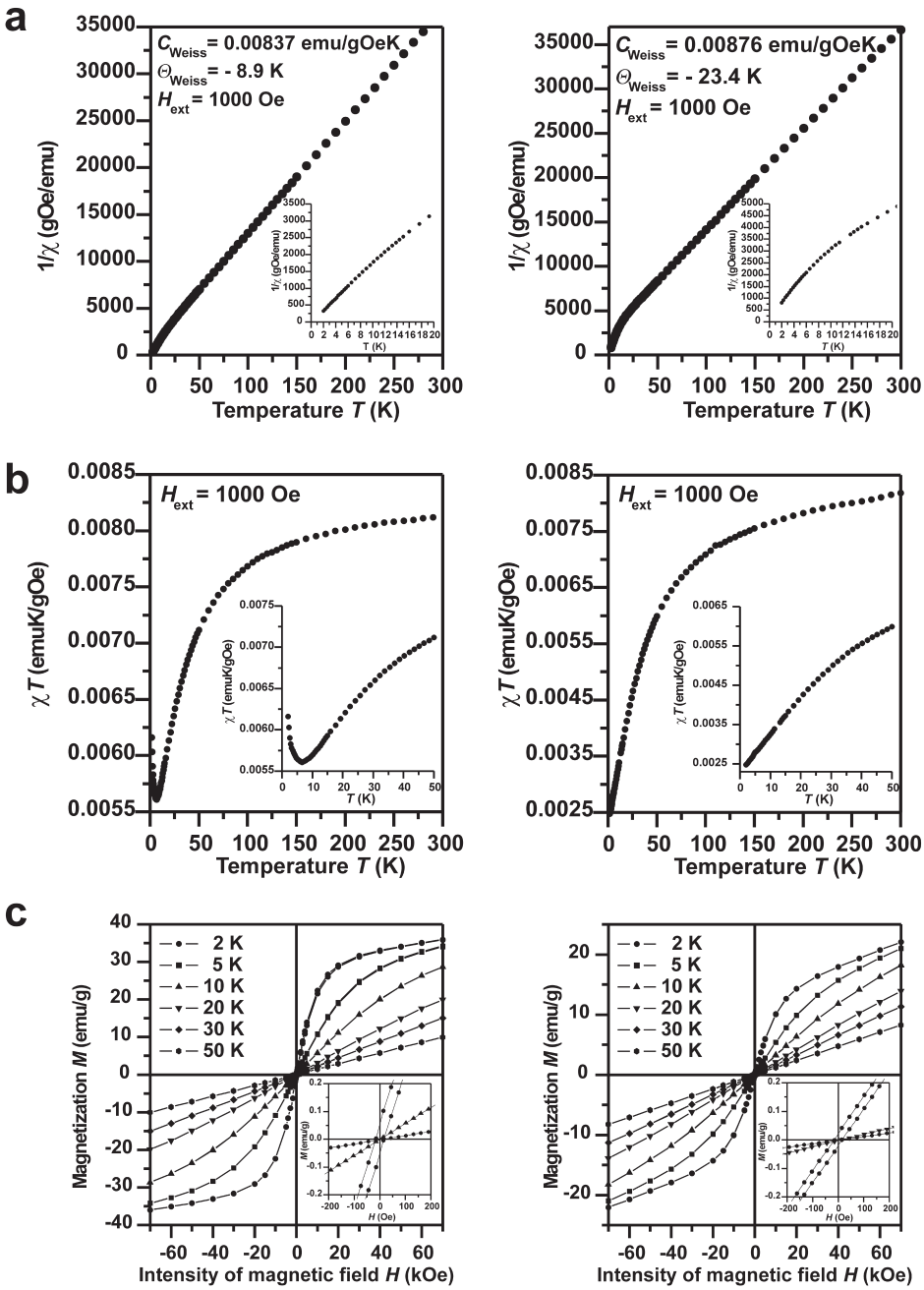

FIGURE 6. The results of magnetic measurements of manganaxinite (left) and tinzenite (right). (**a**) Inverse temperature dependence of magnetic mass susceptibility (χ) with an inset of low-temperature region 0–20 K. (**b**) Plot of χT vs. T with an inset of low-temperature region 0–50 K. (**c**) Field dependence of the magnetization at selected temperatures with an inset of the hysteresis loop near the origin.

romagnetic nature taking place between Mn ions. This is also evident from the profile of χT vs. T curve in the temperature interval from 10 to 300 K (see Fig. 6b, left), being typical of antiferromagnetic materials for which the product of χT decreases with falling temperature (Blundell 2001). In contrast to ferroaxinite, no other significant types of magnetic interactions have been identified in manganaxinite. Hence, there is evidently negligible or no contribution of substituted Fe, being mostly in the Fe^{3+} form at the Z1 site. The hysteresis loop measured at 2 K displays some saturation at the highest applied field of 70 kOe, probably as a result of strong antiferromagnetic interactions (see Fig. 6c, left). The coercive field of 17 Oe is similar to that of ferroaxinite. However, the near saturation of the sample implies that below its magnetic transition temperature, manganaxinite does not order in a purely antiferromagnetic manner. Thus, the coupled antiparallel magnetic moments do not cancel each other due to their different magnitudes, leaving a net magnetization in the structure. The manganaxinite exhibits uncompensated

antiferromagnetic (i.e., ferrimagnetic) ordering of the magnetic moments below the transition temperature. Above 10 K, no hysteresis is observed as all magnetic moments behave paramagnetically. Combining hysteresis loops with the profile of χT vs. T curve, one can deduce that the transition to a magnetically ordered state takes place at about 8 K.

As in the case of manganaxinite, the dominant source of magnetism in the tinzenite sample is the Mn atoms and the interactions among them. Compared to manganaxinite, tinzenite contains more Mn apfu and thus a stronger antiferromagnetic response is expected. This is reflected in the Weiss temperature, which was calculated as –23.4 K (see Fig. 6a, right). Furthermore, the prevalence of strong antiferromagnetic interactions is seen in the plot of χT vs. T (see Fig. 6b, right), where the product of χT increases with increasing temperature across the entire temperature interval. The hysteresis loop at 2 K yields a coercive field of 15 Oe and does not show any indication of saturation at the highest applied magnetic fields. Additionally, at the strongest applied magnetic fields, the sample magnetization values obey a linear relationship (see Fig. 6c, right), which is commonly seen in perfectly aligned antiferromagnetic materials with complete spin balance of sublattice magnetizations. This behavior together with the profile of χT vs. T curve implies that tinzenite orders purely antiferromagnetically at low temperatures, in contrast to magnanaxinite for which an uncompensated antiferromagnetic low-temperature magnetic regime was observed. As temperature increases, the shape of the hysteresis loops changes (see Fig. 6c, right) and at temperatures >20 K, the loops resemble paramagnetic materials with no coercive field. This result indicates that the magnetic transition temperature of tinzenite is slightly above 10 K. Analogous to ferroaxinite, other magnetic ions (e.g., Fe^{2+} and Fe^{3+}), whose presence in very low concentrations has been detected from both EMPA and Mössbauer spectroscopy, may participate in the overall magnetic behavior of both magnanaxinite and tinzenite at low temperatures, although their direct manifestation has not been clearly observed in the magnetic measurements.

Let us now turn back to the heat-capacity data, where ferroaxinite has a C_P minimum at around 6 K with a local maximum below 2 K, whereas manganaxinite and tinzenite display unusually high C_P at 5 K with a concave shape of the C_P-T data with a Schottky-like maximum between 5 and ~12 K (see Figs. 3 and 4). These anomalies can be correlated with some of the features observed in the temperature-dependent magnetic measurements. For manganaxinite and tinzenite, the C_P anomalies correlate well with antiferromagnetic ordering at 8 and 10 K, respectively. However, it is difficult to distinguish between the magnetic ordering of Mn ions into an antiferromagnetic state and a typical Schottky anomaly, possibly arising from electronic effects (i.e., crystal-field splitting of the ground state of Mn ions; cf. Gopal 1966; Hemingway and Robie 1984). For a better understanding of the low-temperature C_P data of manganaxinite and tinzenite, investigation of specific heat under various applied magnetic fields would give an unambiguous interpretation (cf. Lopez et al. 2002). For ferroaxinite, the peak for the heat-capacity anomaly was not detected in this work as the maximum is at or below 2 K. Indeed, strong ferromagnetic interactions at temperatures below 5 K (see Figs. 5b and 5c), may be responsible for the low-temperature C_P anomaly. Moreover, low-temperature magnetic data for magnesioaxinite (not shown) indicates that there is no magnetic transition in the temperature range from 2 to 300 K, and hence no contribution to the low-temperature C_P data. The discrepancy in the temperature where calorimetric and magnetic anomalies take place may arise from several sources, including nonequivalence of the methods employed (magnetization has a vector character, whereas heat capacity is a scalar).

Acknowledgments

We are indebted to R. Škoda, B. David, and O. Schneeweiss for technical assistance, P. Kašpar, P. Bongaerts, and E.L. Belokoneva for providing the sample, and to R. Zbořil for helpful comments. We thank G.B. Andreozzi, B.M. Moskowitz, and an anonymous reviewer for constructive criticism that significantly improved the manuscript. This work has been supported by research projects of Ministry of Education of Czech Republic, grant numbers MSM6198959218 and MSM0021622412, and by the Austrian Science Fund, under project number P15880-N11.

References cited

Andreozzi, G.B., Lucchesi, S., and Graziani, G. (2000a) Structural study of magnesioaxinite and its crystal-chemical relations with axinite-group minerals. European Journal of Mineralogy, 12, 1185–1194.

Andreozzi, G.B., Ottolini, L., Lucchesi, S., Graziani, G., and Russo, U. (2000b) Crystal chemistry of the axinite-group minerals: A multi-analytical approach. American Mineralogist, 85, 698–706.

Andreozzi, G.B., Lucchesi, S., Graziani, G., and Russ, U. (2004) Site distribution of Fe^{2+} and Fe^{3+} in the axinite mineral group: New crystal-chemical formula. American Mineralogist, 89, 1763–1771.

Anovitz, L.M. and Hemingway, B.S. (1996) Thermodynamics of boron minerals: summary of structural, volumetric and thermochemical data. In E.S. Grew and L.M. Anovitz, Eds., Boron: Mineralogy, Petrology and Geochemistry, 33, p. 181–261. Reviews in Mineralogy, Mineralogical Society of America, Chantilly, Virginia.

Basso, R., Della Giusta, A., and Vlaic, G. (1973) The crystal structure of tinzenite. Periodico di Mineralogia—Roma, 42, 369–379.

Belokoneva, E.L., Pletnev, P.A., and Spiridomov, E.M. (1997) Crystal structure of low-manganese tinzenite (severingite). Crystallography Reports, 42, 934–937.

Belokoneva, E.L., Goryunova, A.N., Pletnev, P.A., and Spiridonov, E.M. (2001) Crystal structure of high-manganese tinzenite from the Falotta deposit in Switzerland. Crystallography Reports, 46, 30–32.

Blundell, S. (2001) Magnetism of Condensed Matter. Oxford University Press, U.K.

Dachs, E. and Bertoldi, C. (2005) Precision and accuracy of the heat-pulse calorimetric technique: low-temperature heat capacities of milligram-sized synthetic mineral samples. European Journal of Mineralogy, 17, 251–259.

Dachs, E. and Geiger, C.A. (2006) Heat capacities and entropies of mixing of pyrope-grossular ($Mg_3Al_2Si_3O_{12}$-$Ca_3Al_2Si_3O_{12}$) garnet solid solutions: A low-temperature calorimetric and a thermodynamic investigation. American Mineralogist, 91, 894–906.

Dachs, E., Geiger, C.A., von Seckendorff, V., and Grodzicki, M. (2007) A low-temperature calorimetric study of synthetic (forsterite + fayalite) {(Mg_2SiO_4 + Fe_2SiO_4)} solid solutions: An analysis of vibrational, magnetic, and electronic contributions to the molar heat capacity and entropy of mixing. Journal of Chemical Thermodynamics, 39, 906–933.

Deer, W.A., Howie, R.A., and Zussman, J. (1997) Rock-Forming Minerals, vol. 1B, Disilikates and Ring Silikates, 3rd edition. Longman, London.

Dubé, B. and Guha, J. (1993) Factors controlling the occurrence of ferro-axinite within archean gold copper-rich quartz veins—Cooke mine, Chibougamau area, Abitibi greenstone-belt. Canadian Mineralogist, 31, 905–916.

Filip, J., Kolitsch, U., Novák, M., and Schneeweiss, O. (2006) The crystal structure of near-end-member ferroaxinite from an iron-contaminated pegmatite at Malesov, Czech Republic. Canadian Mineralogist, 44, 1159–1170.

Gmelin, A. (1969) Thermal properties of alcaline-earth-oxides. Zeitschrift fur Naturforschung Section A-A Journal of Physical Science, 24a, 1794–1800.

Gopal, E.S.R. (1966) Specific heats at low temperatures, 240 p. Heywood Books, London.

Grew, E.S. (1996) Metamorphic Borosilicates and Boron in Metamorphic Minerals. In E.S. Grew and L.M. Anovitz, Eds., Boron: Mineralogy, Petrology and Geochemistry, 33, 387–502. Reviews in Mineralogy, Mineralogical Society of America, Chantilly, Virginia.

Grønvold, F. and Westrum, E.F., Jr. (1958) α-ferric oxides: Low temperature heat capacity and thermodynamic functions. Journal of the American Chemical Society, 81, 1780–1783.

Hemingway, B.S. and Robie, R.A. (1984) Heat capacity and thermodynamic functions for gehlenite and staurolite: with comments on the Schottky anomaly in

the heat capacity of staurolite. American Mineralogist, 69, 307–318.
Ito, T. and Takéuchi, Y. (1952) The crystal structure of axinite. Acta Crystallographica, 5, 202–208.
Ito, T., Takéuchi, Y., Ozawa, T., Ariki, T., Zoltai, T., and Finney, S.S. (1969) The crystal structure of axinite revised. Proceedings of the Japan Academy, 45, 490–494.
Jobbins, E.A., Tresham, A., and Young, B.R. (1975) Pale blue axinite from East Africa. The Journal of Gemmology, 14, 368–375.
Lopez, J., de Lima, O.F., Lisboa-Filho, P.N., and Araujo-Moreira, F.M. (2002) Specific heat at low temperature and magnetic measurements in $Nd_{0.5}Sr_{0.5}MnO_3$ and $R_{0.5}Ca_{0.5}MnO_3$ (R = Nd, Sm, Dy, and Ho) samples. Physical Review B, 66, 2144021–2144027.
Lumpkin, G.R. and Ribbe, P.H. (1979) Chemistry and physical properties of axinites. American Mineralogist, 64, 635–645.
Lutterotti, L., Matthies, S., and Wenk, H.R. (1999) MAUD: a friendly Java program for material analysis using diffraction. IUCr: Newsletter of the C_PD, 21, 14–15.
Mazdab, F.K., Anovitz, L.M., and Hemingway, B.S. (1994) Heat capacities and derived thermodynamic functions for several borosilicate and borate minerals, 74 p. University of Arizona, Tucson.
Merlet, C. (1994) An accurate computer correction program for quantitative electron-probe microanalysis. Mikrochimica Acta, 114, 363–376.
Milton, C., Hildebrand, F.A., and Sherwood, A.M. (1953) The identity of tinzenite with manganoan axinite. American Mineralogist, 38, 1148–1158.
Novák, M. and Filip, J. (2002) Ferroan magnesioaxinite from hydrothermal veins at Lazany, Brno Batholith, Czech Republic. Neues Jahrbuch Fur Mineralogie-monatshefte, 9, 385–399.
Ozaki, M. (1972) Chemical composition and occurrence of axinite. Kumamoto Journal of Science: Geology, 9, 1–34.
Pringle, I.J. and Kawachi, Y. (1980) Axinite mineral group in low-grade regionally metamorphosed rocks in southern New Zealand. American Mineralogist, 65, 1119–1129.
Robie, R.A. and Hemingway, B.S. (1985) Low-temperature molar heat-capacities and entropies of MnO_2 (pyrolusite), Mn_3O_4 (hausmannite), and Mn_2O_3 (bixbyite). Journal of Chemical Thermodynamics, 17, 165–181.
Sanero, E. and Gottardi, G. (1968) Nomenclature and crystal-chemistry of axinite. American Mineralogist, 53, 1407–1411.
Stølen, S., Glockner, R., Grønvold, F., Atake, T., and Izumisawa, S. (1996) Heat capacity and thermodynamic properties of nearly stoichiometric wustite from 13 to 450 K. American Mineralogist, 81, 973–981.
Woodfield, B., Shapiro, J., Stevens, R., Boerio-Goates, J., Putnam, R., Helean, K., and Navrotsky, A. (1999) Molar heat capacity and thermodynamic functions of $CaTiO_3$. Journal of Chemical Thermodynamics, 31, 1573–1583.
Žák, T. (2001) Updating of the user-interface fitting program "CONFIT" to "CONFIT2000." Czechoslovak Journal of Physics, 51, 735–742.

Manuscript received April 23, 2007
Manuscript accepted September 30, 2007
Manuscript handled by Joshua Feinberg

Appendix A: Heat capacity extrapolation to 0 K

For manganaxinite and tinzenite, the lattice part of the heat capacity was evaluated by applying a function of the form

$$C_P = 3R[m \cdot D(\theta_D) + n \cdot E(\theta_E)] + A_1 \cdot T + A_2 \cdot T^2$$

to the heat-capacity data above 25 K (e.g., Woodfield et al. 1999). In this expression, R is the gas constant, m and n are coefficients of Debye and Einstein functions, respectively, and A_1 and A_2 are coefficients of T and T^2 terms that constitute an approximation to the difference $C_P - C_V$.

The corresponding fit values are:

Manganaxinite: $m = 14.51 \pm 0.07$, $\theta_D = 360 \pm 4$ K, $n = 20.5 \pm 0.4$, $\theta_E = 657 \pm 4$ K, $A_1 = 0.163 \pm 0.003$ J/(K^2·mol), $A_2 = 0.00134 \pm 0.00007$ J/(K^3·mol).

Tinzenite: $m = 12.49 \pm 0.08$, $\theta_D = 355 \pm 4$ K, $n = 18.2 \pm 0.3$, $\theta_E = 626 \pm 4$ K, $A_1 = 0.436 \pm 0.004$ J/(K^2·mol), $A_2 = 0.00117 \pm 0.00007$ J/(K^3·mol).

With these values, the measured PPMS heat capacities of manganaxinite and tinzenite above 25 K can be well reproduced. The difference $C_{P\ \mathrm{measured}} - C_{P\ \mathrm{lattice}}$ was then fit to a Schottky anomaly with an analogous expression as used by Dachs et al. (2007) for the case of Fe-Mg olivines.

The contributions of the so derived functions $C_{P\ \mathrm{lattice}} + C_{P\ \mathrm{Schottky}}$ between 0 and 5 K to the standard entropies amount to 1.88 J/(mol·K) for manganaxinite and to 4.28 J/(mol·K) for tinzenite and have been added to the calorimetric entropies calculated for the temperature interval 5–298.15 K from the PPMS C_P values.